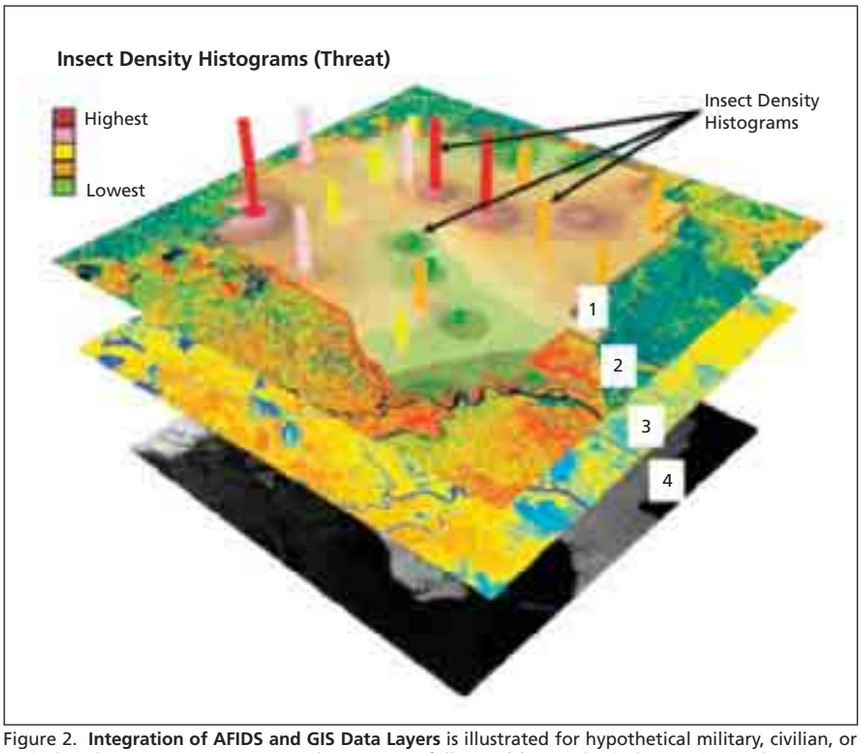

Figure 2. **Integration of AFIDS and GIS Data Layers** is illustrated for hypothetical military, civilian, or agricultural pest management. Data layers are as follows: (1) Hypothetical AFIDS insect density contours (histograms = threat intensity); (2) STAR-3i radar imagery; (3) ASTER Normalized Difference Vegetative Index; and (4) LIDAR digital terrain.

(bottom panel). All AFIDS data are preprocessed in the field with the use of a laptop computer equipped with LabVIEW™. The AFIDS software can be programmed to run continuously or at specific time intervals when insects are prevalent.

A special DC-restored transimpedance amplifier reduces the contributions of low-frequency background light signals, and affords approximately two orders of magnitude greater AC gain than conventional amplifiers. This greatly increases the signal-to-noise ratio and enables the detection of small changes in light intensity. The AFIDS light source consists of high-intensity AlGaInP light-emitting diodes (LEDs). The AFIDS circuitry minimizes brightness fluctuations in the LEDs and when integrated with an integrating sphere, creates a diffuse uniform light field. The insect wing beats isotropically scatter the diffuse light in the sphere and create wing-beat signatures that are detected by the sensor. This configuration minimizes variations in signal associated with insect flight orientation.

Preliminary data indicate that AFIDS has sufficient sensitivity and frequency-measuring capability to differentiate between male and female mosquitoes (Figure 1, bottom panel) and fruit flies (data not shown). Similar studies show that AFIDS can be utilized to detect discrete differences between two mosquito species, *Aedes aegypti* and *Aedes albopictus*.

When fully deployable, a wireless network of AFIDS monitors could be used in combination with other remotely sensed data and visually displayed in a geographic information system (GIS) to provide real-time surveillance (see Figure 2). More accurate and sensitive insect population forecasts and effective rapid response and mitigation of insect issues would then be possible.

This work was done by Timi Vann of Stennis Space Center and Jane C. Andrews, Dane Howell, and Robert Ryan of Lockheed Martin Corp.

Inquiries concerning rights for the commercial use of this invention should be addressed to the Intellectual Property Manager, Stennis Space Center, (228) 688-1929. Refer to SSC-00192.

Calligraphic Poling of Ferroelectric Material

Arbitrary patterns can be written relatively easily and inexpensively.

NASA's Jet Propulsion Laboratory, Pasadena, California

Calligraphic poling is a technique for generating an arbitrary, possibly complex pattern of localized reversal in the direction of permanent polarization in a wafer of $LiNbO_3$ or other ferroelectric material. The technique is so named because it involves a writing process in which a sharp electrode tip is moved across a surface of the wafer to expose the wafer to a polarizing electric field in the desired pattern. The technique is implemented by use of an apparatus, denoted a calligraphic poling machine (CPM), that includes the electrode and other components as described in more detail below.

A capability for forming poling patterns is needed for research on, and development of, photonic devices that exploit the nonlinear optical properties of ferroelectric crystals. Specific poling structures in ferroelectric crystals can be engineered to variously amplify or suppress these nonlinear optical properties to effect such useful functions as optical switching, modulation, frequency conversion, and frequency filtering.

Outside of industry, poling machines have been available to only a few research laboratories and have been typified by high costs and limited flexibility. Prior poling techniques and machines are suitable for generating relatively simple patterns (e.g., straight lines) but are not suitable for generating the arbitrary patterns required in some applications. Each of the prior techniques involves one or more of the following: expensive fabrication of electrically conductive masks, expensive holograms, a cleanroom, high vacuum, and high temperature. In contrast, a CPM operates in air at room temperature with equipment readily available in a typical laboratory; hence, calligraphic poling costs less than does poling by the prior techniques.

In a CPM (see figure), the wafer to be poled is placed in the *x*–*y* (horizontal)

plane on a smooth, flat substrate that serves as a lower electrode. Typically, the wafer is a crystal of $LiNbO_3$ or other ferroelectric material that is *z*-cut. [In this case, "*z*-cut" signifies that the polarization axis of the wafer is perpendicular to its broad faces and thus coincides with the *z* (vertical) axis when the wafer is placed on the substrate]. A thin layer of saltwater is placed between the substrate and the wafer to ensure electrical contact between the nominally planar wafer and substrate surfaces. The thin layer of saltwater also serves to mechanically bind the wafer temporarily to the substrate. The electrode has a tungsten tip 0.5 μm wide and is biased at a suitable potential with respect to the substrate (typically, ≈1.5 kV for a 100-μm-thick $LiNbO_3$ crystal). The writing electrode is mounted on an *x*–*y* translation stage, which is used to move the electrode across the wafer surface in the desired pattern.

By varying the magnitude and duration of the applied voltage in conjunction with the motion or stationarity of the electrode, one can exert some control over the sizes and shapes of the ferroelectric domains. For example, it was found that smooth lines having widths of the order of a few microns could be formed by applying potentials between 0.8 and 1.8 kV for times of the order of 10 s while the pen was moving, as illus-

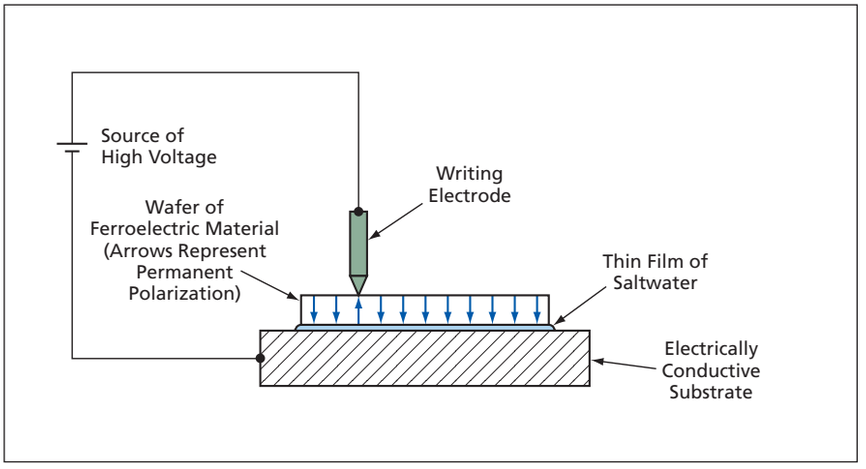

Figure 1. A **Sharp Electrode** applies a strong electric field to effect localized poling of the wafer. Used like a pen, the electrode is moved across the wafer to write a poling pattern.

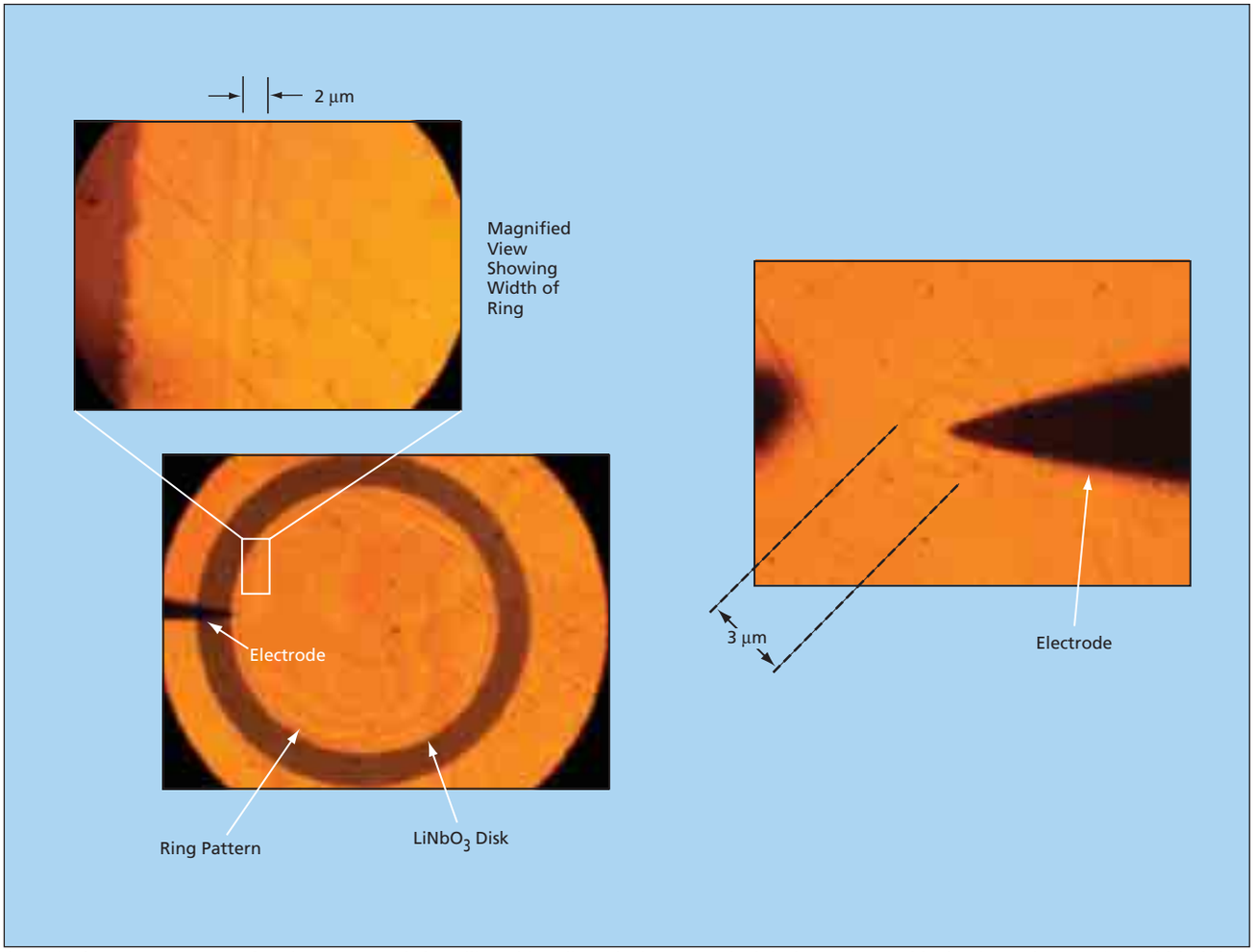

Figure 2. **These Are Two Examples** of patterns made by calligraphic poling. The images at the left show a 2-μm-wide ring formed on a 100-μm-thick $LiNbO_3$ disk at a potential of 1.8 kV applied during a writing time of 10 s. The image at the right shows a 3-μm-wide hexagonal domain formed on a 120-μm-thick $LiNbO_3$ crystal by use of a 2.5-kV bias applied to a stationary electrode for 1.5 s.

trated in the left part of the figure. For another example, it was found that potentials between 2 and 3 kV applied for times <2 s while the electrode was held stationary yield hexagons (a consequence of the crystalline structure of $LiNbO_3$), as illustrated in the right part of Figure 2.

Among the advantages of calligraphic poling is that it is possible to visually observe the domains in ordinary (that is, non-polarized) light as they are being formed. Light incident from above along the *z*-axis travels through the wafer and is reflected from its bottom surface. The poling electric field magnifies the gradient in the index of refraction between a +*z*- and –*z*-poled region to such an extent as to give rise to a dark outline, coinciding with the boundary between the regions, that is visible in the reflected light when viewed from above through a conventional optical microscope. In addition, it is possible to view the domains nondestructively after they have been formed, because a potential sufficient to generate the dark outline (typically 200 V) is much smaller than the domain-reversal potential.

This work was done by Makan Mohageg, Dmitry Strekalov, Anatoliy Savchenkov, Adrey Matsko, Lute Maleki, and Vladimir Iltchenko of Caltech for NASA's Jet Propulsion Laboratory.

In accordance with Public Law 96-517, the contractor has elected to retain title to this invention. Inquiries concerning rights for its commercial use should be addressed to:

Innovative Technology Assets Management
JPL
Mail Stop 202-233
4800 Oak Grove Drive
Pasadena, CA 91109-8099
(818) 354-2240
E-mail: iaoffice@jpl.nasa.gov

Refer to NPO-41566, volume and number of this NASA Tech Briefs *issue, and the page number.*

Blackbody Cavity for Calibrations at 200 to 273 K

Care must be taken to ensure high emissivity to minimize error.

Stennis Space Center, Mississippi

A laboratory blackbody cavity has been designed and built for calibrating infrared radiometers used to measure radiant temperatures in the range from about 200 to about 273 K. In this below-room-temperature range, scattering of background infrared radiation from room-temperature surfaces could, potentially, contribute significantly to the spectral radiance of the blackbody cavity, thereby contributing a significant error to the radiant temperature used as the calibration value. The spectral radiance error at wavelength λ is given by

$$[1 - \varepsilon(\lambda)][B(T_c,\lambda) + B(T_a,\lambda)],$$

where $\varepsilon(\lambda)$ is the effective spectral emissivity of the cavity, $B(T,\lambda)$ is the ideal spectral radiance of a body at absolute temperature T according to Planck's radiation law, T_c is the temperature in the cavity, and T_a is the ambient temperature. Examining the above expression shows that by making $\varepsilon(\lambda)$ as close as possible to unity, one can minimize the spectral-radiance error and the associated radiant-temperature error. For example, it has been calculated that to obtain a radiant-temperature error of 1 K or less at a cavity temperature of 200 K, ambient temperature of 300 K, and wavelength of 6 μm, one has $\varepsilon(\lambda)>0.999$ (see Figure 1). A 1 K radiant-temperature error is more than sufficient for atmospheric and cloud studies, which is a common application of infrared radiometers.

The present blackbody cavity is of an established type in which multiple reflections from a combination of conical and cylindrical black-coated walls (see Figure 2) are exploited to obtain an effective emissivity greater than the emissivity value of the coating material on a flat exposed surface. The coating material in this case is a flat black paint that has an emissivity of approximately 0.91 in the thermal spectral range and was selected over other, higher-emissivity materials because of its ability to withstand thermal cycling. We found many black coatings cracked and flaked after thermal cycling due to differences in the coefficient of expansion. On the basis of theoretical calculations, the effective emissivity is expected to approach 0.999.

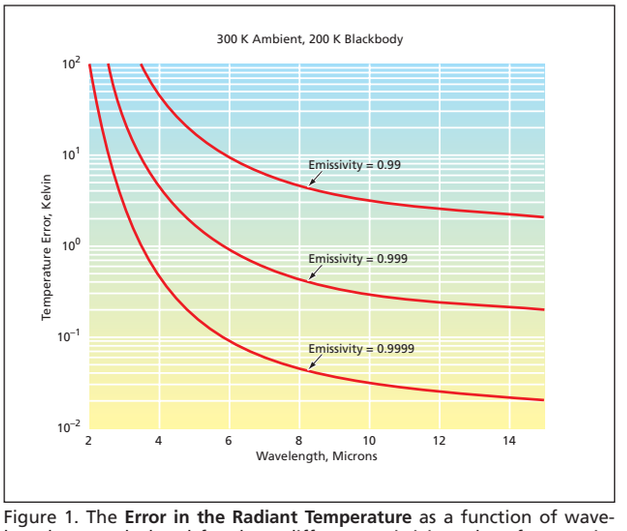

Figure 1. The **Error in the Radiant Temperature** as a function of wavelength was calculated for three different emissivity values for a cavity temperature of 200 K and ambient temperature of 300 K.

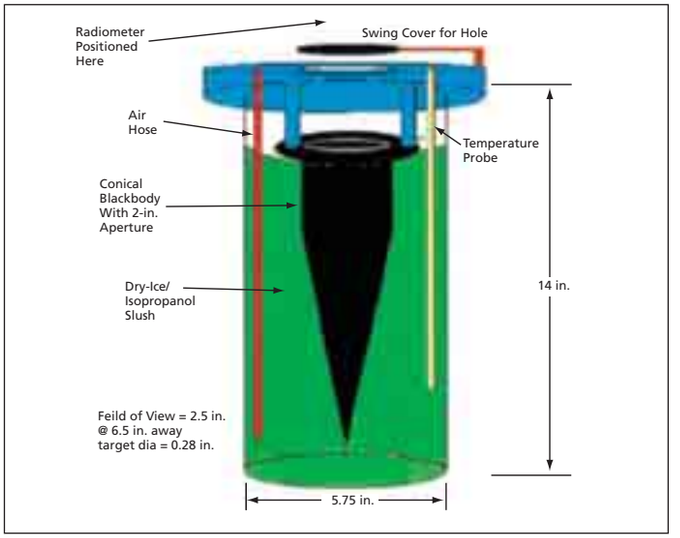

Figure 2. The **Blackbody Cavity** has a shape and size chosen as a compromise among maximizing the number of internal reflections, maximizing effective emissivity out to an acceptably large radius, and keeping the cone short enough to fit in a Dewar flask, as shown.